2019-11

Mechanical properties and tribological behaviour of electroless NiPCu coatings on corrosion-resistant alloys under ultrahigh contact stress with sprayed nanoparticles

MENG, MAOZHOU

10.1016/j.triboint.2019.06.031
Tribology International
Elsevier

Tribological behaviour of electroless Ni-P-Cu coatings on corrosion-resistant alloys under ultrahigh contact stress with sprayed nanoparticles

Maozhou Meng[1, 2], Andrew Leech[3], Huirong Le[1*]

[1]School of Mechanical Engineering and Building Environment, University of Derby, UK

[2]School of Engineering, Plymouth University, UK

[3]Tubular Connections Ltd, Scotland, UK

*Corresponding author: Huirong Le - h.le@derby.ac.uk

Abstract

Threaded components manufactured from corrosion resistant alloys (CRA's) are vulnerable to galling when compared with like components manufactured from carbon steel. This paper develops a test matrix to systematically investigate the tribological performance of electroless nickel phosphorous coatings on CRA's when subjected to various loading regimes (1.5GPa and 2GPa Hertzian contact stress). Samples manufactured from 28Cr stainless steel were shot-peened in a shot-blasting cabinet for various periods prior to being coated using the electroless coating method. The coefficient of friction (CoF) of different coating systems was evaluated by a friction test rig which generated extremely high contact pressures via sliding cross-pin method. Various wet and dry lubricants were utilised to examine tribological performance, furthermore the adhesion strength of the coatings was investigated by a bond and pull-off method. Microscopic observations indicated a gradual surface modification due to various peening times resulting in an optimised surface roughness. The study has shown a significant reduction in CoF for electroless nickel phosphorous coatings due to shot-peening treatments, particularly when tested without the use of conventional wet lubricants. The study has also shown a linear relationship between CoF and contact stress for 'makeup' (loading) and 'breakout' (unloading) regimes.

Keywords: Electroless nickel coating; corrosion resistant alloys; adhesion; friction; galling

1. Introduction

Iron-based corrosion resistance alloys (CRA's) contain high levels of chromium (Cr), nickel (Ni) and molybdenum (Mo), which provide long term resistance to corrosion for many components such as valves, tubes, vessels and heat exchangers exposed to challenging environments where high temperature/pressure combined with CO_2, H_2S, sulphur and chlorides[1-3]. In such hazardous environments other materials subject to pitting and crevice corrosion easily, for instance, carbon steels present very high corrosion rates[4, 5].

High content of nickel within CRA's ensures an excellent resistance to stress-corrosion cracking (SCC), furthermore CRA's resistance to environmental corrosion is the result of the passivation of chrome forming a transparent oxide film on the surface. In general, CRA's having higher chrome content present lower corrosion rate because this passive film is self-repairing if it is scratched or removed. In the previous publications[6, 7], Craig provided guidance for selection of different types of CRA's for specific environments.

Although threaded components manufactured from CRA's exhibit excellent corrosion resistance, they have a higher galling propensity when compared with components manufactured from carbon steel. There are ways to reduce the risk of galling, e.g. (1) making the hardness difference between the contact pair a preferred range; (2) controlling the surface roughness of contact surfaces -- highly polished surfaces (Ra<0.25 μm) or very rough surfaces (Ra >1.5 μm) tend to have a higher galling propensity and (3) reducing friction by selecting a suitable lubricant.

To address these problems, various coatings and lubricants have been developed, of which the electrolytic copper plating combined with API dope (wet lubricant) has been widely used on threaded connections. API dope was originally developed to form a seal in threaded connections, further use confirmed the heavy metal content worked well as an anti-galling medium particularly when used in conjunction with electrolytic copper plating. Such anti-galling systems work well when used on materials with a high galling propensity. The heavy metal content within previous API dope formulations was considered to have an adverse effect on the environment which has led to the development of other none toxic lubricants for the assembly of various equipment.

Electroless nickel phosphorous (Ni-P-Cu) coating is well known for its corrosion resistance, particularly when copper is added enhancing the coatings resistance to hazardous environments, such as high concentration of sodium chloride (NaCl) or hydrochloride acid

(HCl) [8, 9]. The electroless deposition is an autocatalytic method without the use of an external electric power source, therefore it is possible to deposit a uniform even coating on substrates with complex geometry since there is no variation in current density. This is beneficial for certain components such as threaded connections that are designed with very close tolerances.

The electroless process relies on the presence of a reducing agent (sodium hypophosphite or borohydride), which reduces the nickel ions at a relatively high temperature (e.g. 70-90 °C). Currently, there is no agreement to explain the chemical reaction mechanisms of the electroless nickel coating [10, 11], however the most accepted mechanisms are that the atomic hydrogen (H_{ads}) is released as the result of the catalytic dehydrogenation of hypophosphite molecule adsorbed at sample's surface, while the adsorbed active hydrogen reduces nickel ion at the surface of the catalyst.

$$
\begin{aligned}
&H_2PO_2^- + H_2O \rightarrow HPO_3^{2-} + H^+ + 2H_{ads} \\
&Ni^{2+} + 2H_{ads} \rightarrow Ni\downarrow + 2H^+ \\
&2H_{ads} \rightarrow H_2\uparrow \\
&H_2PO_2^- + H_{ads} \rightarrow P\downarrow + H_2O + OH^-
\end{aligned}
\qquad (1)
$$

Free hydrogen ions (H^+) are produced during this chemical reaction, therefore organic salts (i.e. sodium citrate, ammonia acetate) are added as a buffer to prevent the PH value from decreasing too quickly. The organic salts also act as a complexing agent, maintaining a proper amount of free nickel ions in the solution to make the deposition rate controllable.

Apart from the anti-corrosion properties, electroless nickel coating exhibits excellent tribological properties. According to a statistic[12], the primary uses of electroless nickel coatings are due to their anti-corrosion (30%) and wear resistance (25%) properties. Many tribological tests for electroless nickel coatings have been conducted, such as pin on disc[13], ball on disc[14], block on ring[15], and ring on ring[16]. In the previous reports the electroless nickel coatings were applied on either magnesium/aluminium alloys or mild steel which were benefitted by the superior corrosion resistant properties, however there seems to be lack of systematic investigation of electroless nickel deposition on CRA's.

In this study, electroless nickel phosphorous coatings were successfully deposited on 28Cr stainless steel cylindrical pin samples by using various surface pre-treatment and activation methods. Dry and wet lubricants were applied for tribological testing under intermediate and high contact pressure in a galling and friction rig. The CoF was extracted to evaluate the

friction performance and the wear scars were inspected to estimate the galling resistance. The study has shown a positive effect of the shot-peening process on the tribological properties of the electroless nickel coatings, and a dramatic reduction of CoF was achieved when nanoparticles were applied as a dry lubricant.

2. Sample preparation

The tribological performance of electroless nickel phosphorous coating depend on many factors, such as surface pre-treatment, chemical composition of coating solution, bath temperature and lubricants used. This study developed a test matrix to include such parameters, covering different coating systems and lubricants, as shown in Table 1. Electrolytic copper plating is also shown in the table as a benchmark.

Table 1. Test matrix

Coating	Ni-P	Ni-P-Cu	Cu	
Wet lubricant	API dope			
Dry lubricant	PTFE	WS_2	Tin	Lead

Samples were designed and manufactured into cylindrical pins with a radius of 6 mm and length of 100 mm. The pin samples were treated with various surface pre-treatments, such as shot-peening, mechanical polishing (#600 silicon carbide paper), conventional cleaning, alkaline cleaning with Ultraclean SPX alkaline detergent (Ultrawave®), and nickel strike, then they were immersed into the chemical baths for electroless deposition. The electrolytic copper coating was prepared by the same procedure by replacing the electroless bath with an electrolytic bath.

Shot-peening with spherical austenitic stainless steel beads (Chronital®) was performed within a Sealey SB970 shot blasting cabinet (Sealey, UK) connected to an air compressor (8 bar). Nickel strike is a surface activation process in which a thin layer of pure nickel is deposited on the substrate surface. The nickel strike solution contained 10 wt% HCl and 300 g/L nickel chloride hexahydrate ($NiCl_2 \cdot 6H_2O$), and a current density of 2.1 A/dm^2 was applied to the cylindrical test pins.

Three coating systems were chosen for this study, including electroless nickel phosphorous (Ni-P), electroless nickel phosphorous copper (Ni-P-Cu) and electrolytic copper (Cu). Table 2 gives detailed information of the bath composition of the three coatings.

Table 2. Chemical composition of the three baths

	Chemical	Formular	Amount(g/L)
Ni-P bath	Nickel sulphate	$NiSO_4 \cdot 6H_2O$	50
	Sodium hypophosphite	$NaH_2PO_2 \cdot H_2O$	30
	Sodium citrate	$HOC(COONa)(CH_2COONa)_2 \cdot 2H_2O$	60
	Ammonium acetate	$CH_3CO_2NH_4$	40
	Thiourea	CH_4N_2S	0.001
Ni-P-Cu bath	Nickel sulphate	$NiSO_4 \cdot 6H_2O$	50
	Sodium hypophosphite	$NaH_2PO_2 \cdot H_2O$	30
	Sodium citrate	$HOC(COONa)(CH_2COONa)_2 \cdot 2H_2O$	60
	Ammonium acetate	$CH_3CO_2NH_4$	40
	Copper sulphate	$CuSO_4 \cdot 5H_2O$	0.5-2
Cu	Copper sulphate	$CuSO_4 \cdot 5H_2O$	200
	Sulfuric acid	H_2SO_4	50

The two electroless baths (Ni-P and Ni-P-Cu) were maintained at a constant temperature of 80 ℃, following 30 minutes a coating film of about 10μm was obtained on the substrate. The chemical reaction of electroless deposition for Ni-P initiated immediately when the CRA test samples were immersed in solution, however the bath was vulnerable to decomposition and black phosphorous sulphide particles spontaneously appeared within the bulk volume of solution. Therefore, a stabilizer, thiourea was added into the Ni-P bath. Ni-P-Cu alloy cannot deposit on CRA's substrate directly, thus an extra activation step was introduced to initialize the chemical reaction. Abner Brenner and Grace Riddell had discussed different activation methods for electroless deposition on different substrates in 1947[17]. In this study, a zinc rod was immersed into the bath and contacted to the substrate for the activation of the electroless deposition of Ni-P-Cu, the copper sulphate content varied between 0.5 to 2 g/L.

3. Mechanical and tribological testing methods

Various mechanical and tribological properties, including adhesion strength, surface roughness and micro-hardness, CoF with different lubricants, were examined to characterize the performance of the three coatings. The wet lubricants used in this study included API dope, and the dry lubricants included tungsten disulphide (WS_2), polytetrafluoroethylene (PTFE), tin and lead. The WS_2 and PTFE were in nanoparticle form and were sprayed on the coatings directly, whilst the tin and lead were deposited film thick onto the substrate by a rotating burnishing method.

A preliminary test was conducted to investigate the effects of copper content in the Ni-P-Cu coatings (copper sulphate concentration varied from 0.5-2 g/L) on the tribological properties, and it was found that such effects were negligible therefore only the results of specific Ni-P-Cu coating prepared from chemical bath with 0.75 g/L copper sulphate concentration were chosen to compare with the other two coatings.

3.1.Adhesion test

The adhesion strength between coating and substrate was measured by an Elcometer 508 digital pull-off adhesion tester (Elcometer, UK), and an acrylic adhesive (3M) was used as a glue bonding the dolly and coating together. This is a versatile and instant glue which can be used to bond a polymer to metal. In order to get the strongest bonding performance, the bonded parts were kept for 24 hours before carrying out the adhesion test. Hydraulic force was applied on a small cylindrical pin which went through the central hole of the dolly causing a relative movement between the coated sample and the dolly. Since the dolly was directly bonded to the substrate coating provided a convenient method for measuring adhesion of the coating with the substrate.

3.2.Surface roughness measurement

The surface profile for various peening periods was evaluated by a confocal laser scanning microscopy (Olympus LEXT OLS3000). The microscope reconstructs 3D structures from the obtained images by collecting sets of images at different depths for the evaluation of surface texture. The surface roughness was measured by a stylus type surface roughness tester (SRT6210, HUATEC, China) which records the position of a diamond probe along a straight path with approximately 4 mm of travel. Three samples were measured to evaluate the surface roughness for each peening period and the average value (R_a) was calculated.

3.3.Micro-hardness test

The hardness testing was performed on a Buehler Omnimet Automaic MHT System (Buehler, UK), which is based on Vickers scale. Samples with coatings were subjected to a 10 g weight and the imprints on the coatings were evaluated for the calculation of micro-hardness. The as-machined substrate was tested as a reference using a 200 g weight. Three measurements were performed and the average value was calculated.

3.4.Friction and galling test

Friction tests were performed to determine the CoF and anti-galling properties of various combinations of wet/dry lubricants and coatings. Fig.1 shows an image of the friction rig and a schematic of the contact imprint of the crossed pins. The test rig was designed so that the two test pins can be mounted on two holders' perpendicular to each other. The top holder was fixed horizontally on two vertical threaded rods, whilst the bottom holder was mounted on a platform with an adjustable gradient which was adjusted using a micrometre screw providing an inclined angle of 5°. Nuts were tightened into the vertical threaded rods so that the top sample holder was pressed downward to make a hard contact with the bottom sample. All samples were made of 28Cr stainless steel. Samples with coating were mounted on the bottom, and the wear scar of top bottom (without coating) was captured by an optical microscope (Olympus SC100, Olympus, UK) for the investigation of anti-galling properties of coatings.

A small initial normal force was applied between the top and bottom test pins by tightening the nuts, and the normal force increased whilst the platform translated via a linear actuator. The sliding speed was controlled at a constant speed of 3 mm/s by LabVIEW (National Instrument, UK), and the total sliding distance of one stroke was 45 mm (one cycle is 90 mm). Three cycles (270 mm) were performed continuously for each test. Tangential and normal forces were recorded continuously by data acquisition to record CoF. The configuration and instrument setup has been described previously [18].

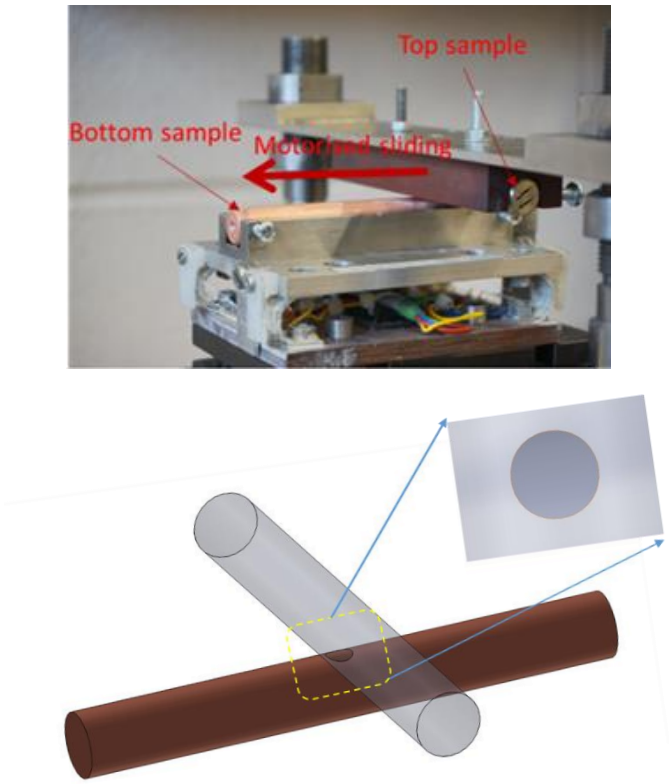

Fig.1. Friction and galling rig test setup

Two loading levels were applied to investigate the frictional and galling properties of the coating / lubricant systems. Hertz theory of contact between elastic bodies was used to evaluate the contact stresses[19]. For crossed cylinders of equal radius R, the maximum and average contact pressure P_0, P_a are given by:

$$P_0 = \frac{1}{\pi}\left(\frac{6FE^*}{R^2}\right)^{1/3} \qquad (2)$$

$$P_a = \frac{2}{3}P_0$$

$$\frac{1}{E^*} = \frac{1-\nu_1^2}{\mathrm{E}_1} + \frac{1-\nu_2^2}{\mathrm{E}_2}$$

Where F is the normal force, E is elastic modulus and ν is the Poisson's ratio. As both top and bottom samples were made of the same material, thus the effective elastic modulus can be simplified as $E^*=0.5E/(1-\nu^2)$. The elastic modulus of 28Cr stainless steel was preliminarily measured as 190GPa in compression and the Poisson's ratio was 0.3. With a normal force of 200 ~ 450 N, the average contact pressure P_a was calculated as 1. 5~2 GPa.

4. Results and discussion

4.1.Shot-peening and surface roughness

The shot-peening was applied for various periods (0, 1, 3, 5 minutes) with a fixed distance of 10 mm between compressor nozzle and pin surface using a shot-peening system. Fig.2 shows 3D surface profile of samples having been subjected to various peening periods. With the increase of shot-peening time the tooling marks were gradually removed, however, the peening process introduced extra roughness when the peening time exceeded a critical value (3-5 minutes), as shown in (d). This is confirmed by the measurement of surface roughness using a cantilever probe, as shown in Fig.3.

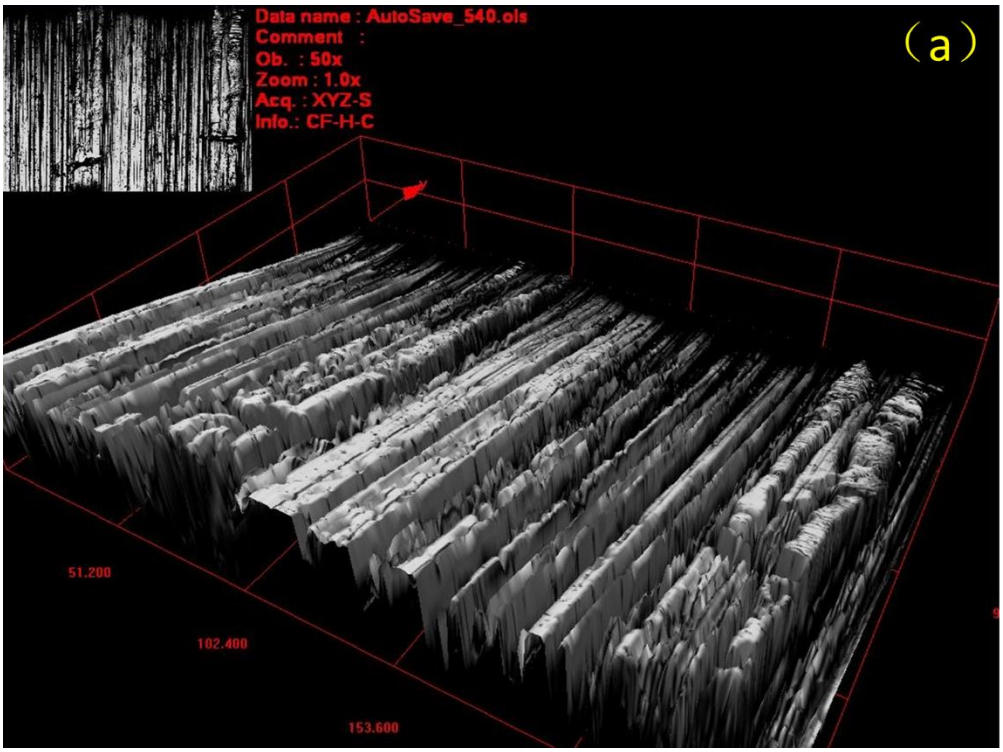

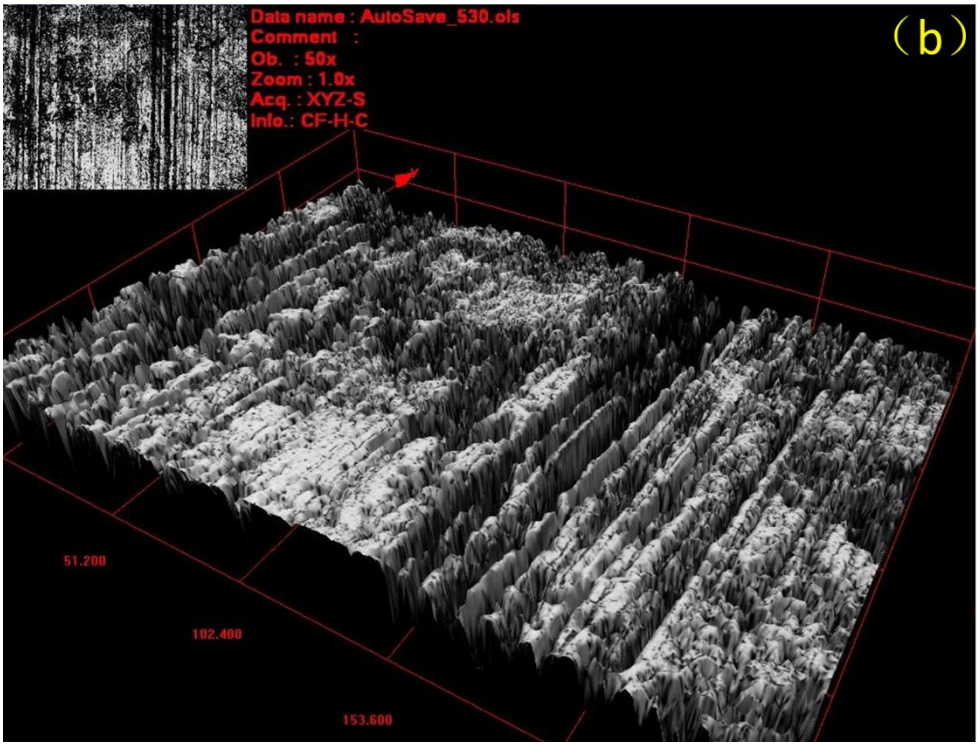

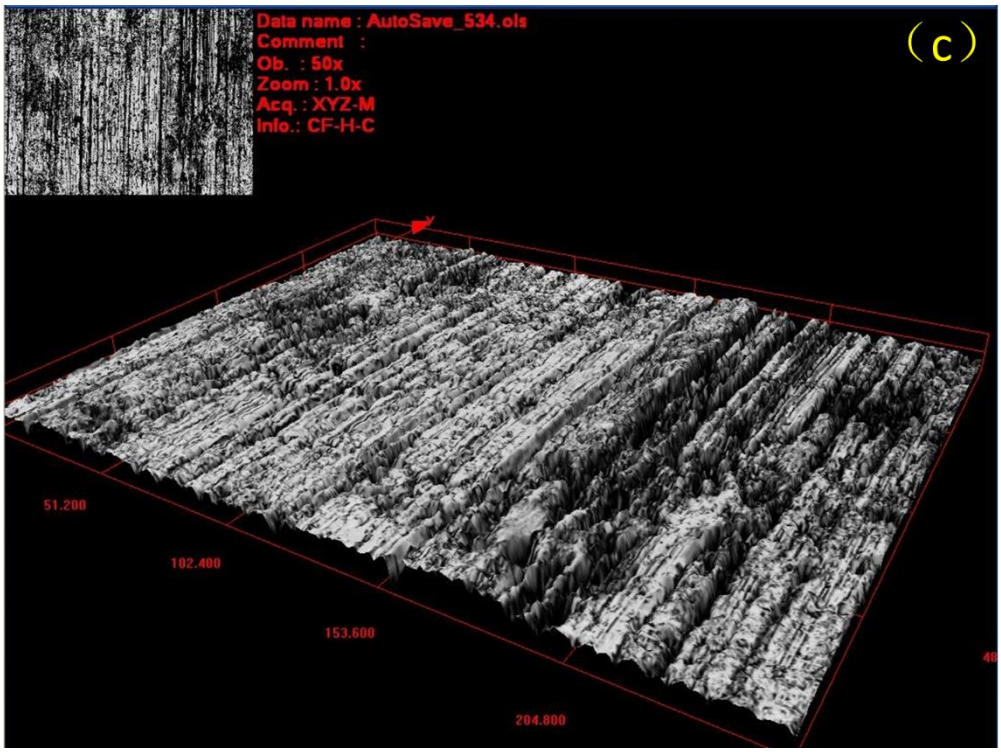

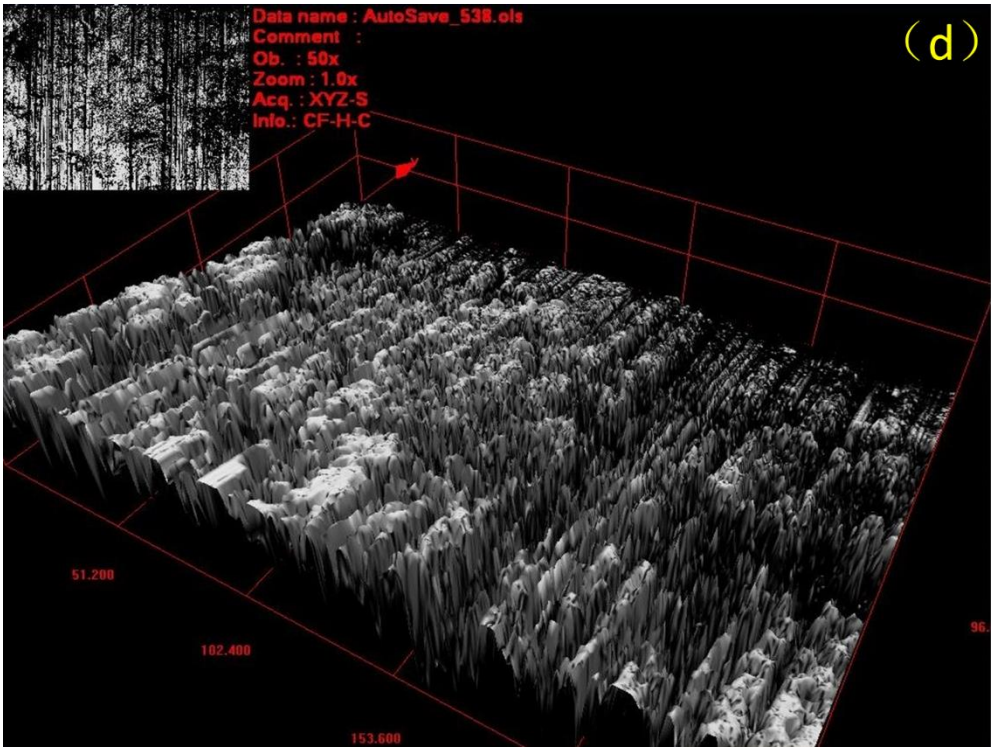

Fig.2. 3D surface profile following various peening periods: (a) as-machined; (b) 1-min peening; (c) 3-min peening; (d) 5-min peening. The tooling marks can be seen clearly from the as-machined sample.

The peening process can not only remove contamination on the surface but also induces surface residual stresses which improves galling resistance. The references [20, 21] have discussed the relationship between shot-peening, surface residual stress and substrate fatigue performance. The craters generated from peening also act as a convenient lubricants trap during sliding contact reducing the amount lubricant being removed from the surface. Fig.3 shows the surface roughness (R_a) for samples with different peening periods. The respective standard variation for each peening condition is also shown in the chart. This measurement indicates an optimized peening configuration for surface modification, therefore 4-minute shot-peening time was chosen for the tribological investigation in this study.

, µm

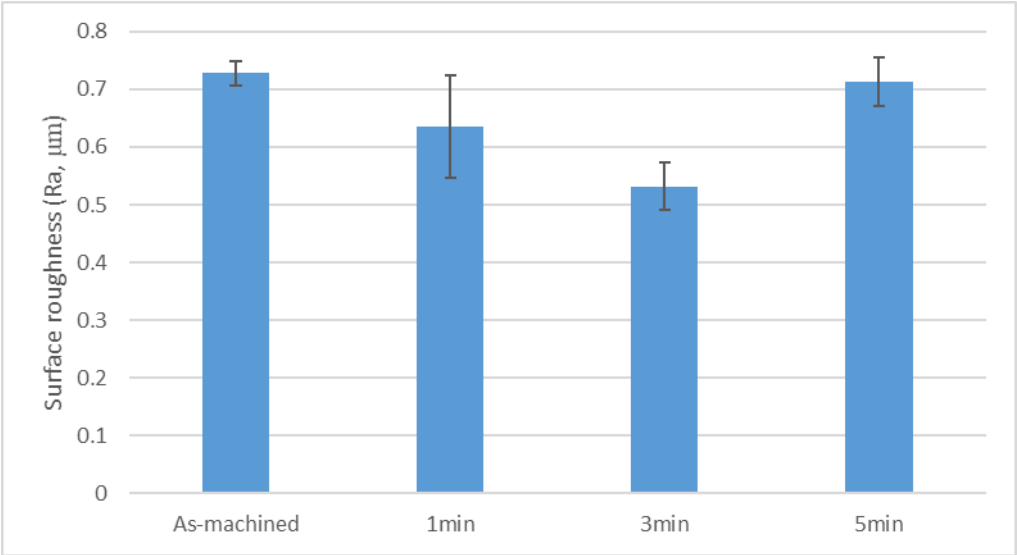

Fig.3. Surface roughness (R_a) for various peening periods

4.2.SEM/EDS inspection and adhesion strength

SEM/EDS (JEOL 7001) was used to assess the element compositions of electroless Ni-P and Ni-P-Cu coatings. The electroless coatings were deposited on flat coupons manufactured from CRA's with a dimension of 40mm x 30mm x 2mm. The element compositions of the two electroless coatings were inspected from a randomly chosen area and the average value of individual element was analysed. Fig.4 shows SEM images of different electroless nickel coatings obtained from various copper sulphate concentration, and the results of element composition are given in Table 3. The Ni-P-Cu coating was prepared by adding various amounts of copper sulphate in the plating bath, from 0.5 to 1.5 g/L. In the figure, 0 g/L represents Ni-P coating. It can be seen from the figure that the Ni-P showed relatively smooth surface profile and very rare coating grains. More coating grains appeared on the surface when the copper sulphate concentration increased from 0 to 1 g/L but decreased again when copper sulphate exceeded 1 g/L.

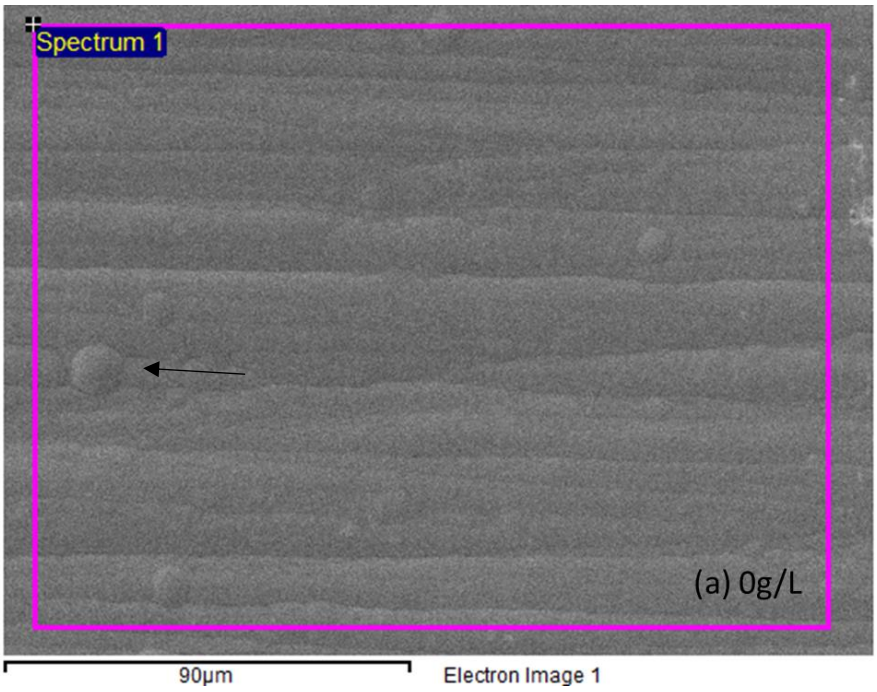

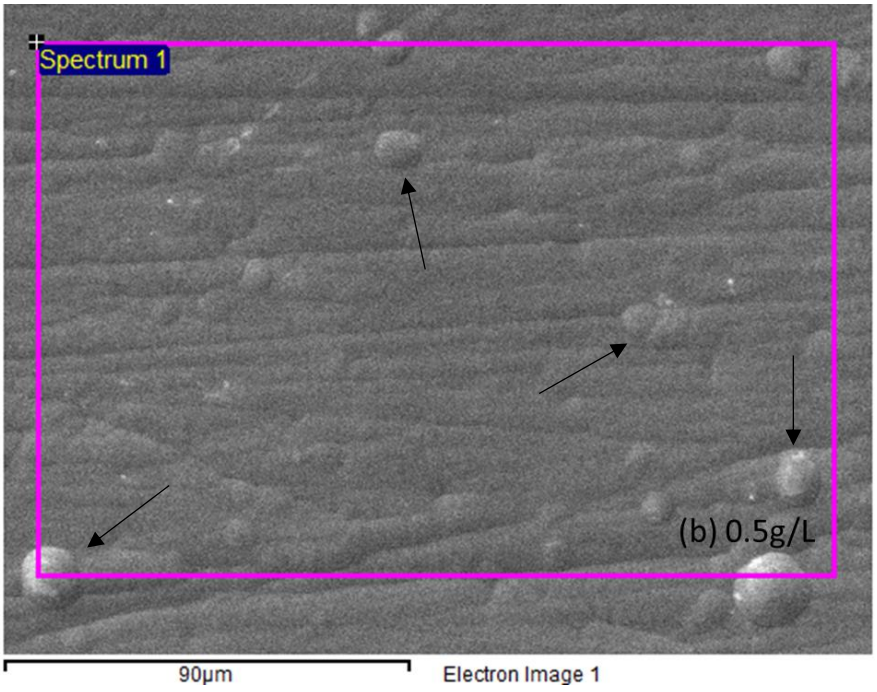

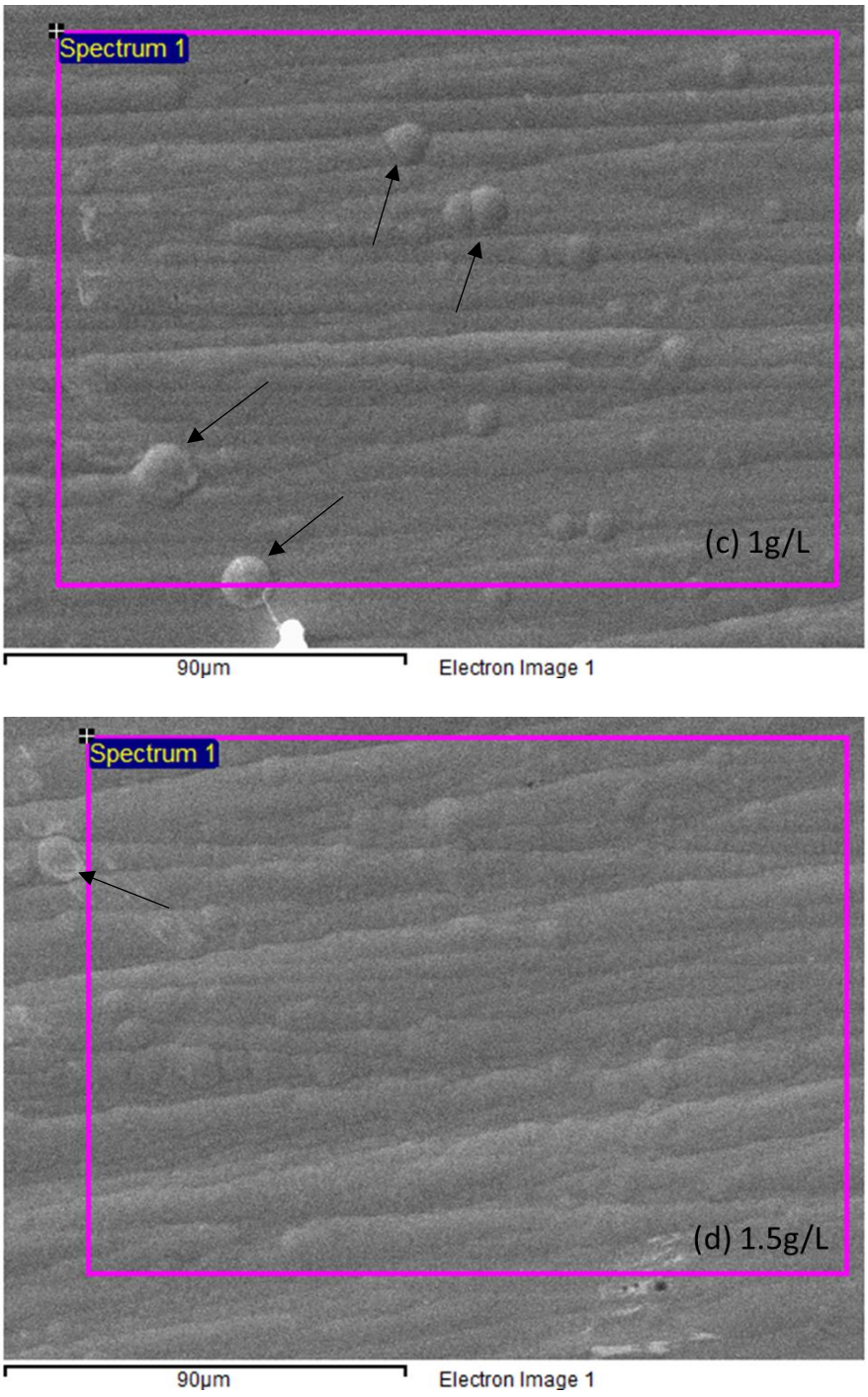

Fig.4. Typical SEM images of electroless nickel coating by various copper sulphate concentration

Because copper is not a catalytic element for such an electroless bath, the Ni-P-Cu bath became increasingly difficult to control when copper content increased within the coating film. The coating film appeared to be a pure copper layer if the electroless Ni-P-Cu bath contained more than 2.5 g/L copper sulphate, and no Ni-P-Cu coating was obtained on the CRA's substrate regardless of activation methods.

Table 3. Element compositions of electroless Ni-P and Ni-P-Cu coatings (wt%)

$CuSO_4.5H_2O$	0 g/L	0.5 g/L	0.75 g/L	1 g/L	1.5 g/L
P	13.26	13.34	12.9	10.84	9.83
Ni	86.74	83.39	82.23	82.61	74.29
Cu	0	3.27	4.87	6.56	15.88

The table shows a trend that with the increase of copper sulphate concentration in the plating bath, both Ni and P content were reduced gradually. Both the Ni^{2+} and Cu^{2+} are complexed by ligands (NH_3, CH_3CH_2COOH) in the chemical bath, and their chemical properties in aqueous solution are altered when they combine with different complexing agent[22, 23]. These two types of ions compete to oxidize the reducing agent (hypophosphite). Compared to nickel ions, copper is much easier to deposit due to a much stronger electrode potential. According to Salvago and Cavallotti[24], copper can be reduced by $H_2PO_2^-$ without P co-deposition, showing the direct intervention of the chemical nature of the metal in the co-deposition reaction, hence the table shows a reduction of phosphorus content.

The industry normally classifies an electroless nickel coating with over 10 wt% phosphorous content as a high phosphorous coating, while the phosphorous coating is mainly controlled by pH value (the higher pH the lower phosphorous content). The electroless nickel coating becomes amorphous and presents relatively lower hardness when phosphorous content is higher than 7 wt%[25], and this controllable hardness can be carefully designed to match the hardness of the contact pair to provide optimized wear and anti-galling properties. Due to the physical barrier of phosphorous and copper within the nickel matrix, coating with high content of phosphorous and copper tends to have better corrosion resistant properties[26]. In literature[27], Parkinson has provided a detailed discussion on properties and applications of electroless nickel coatings.

Coatings with poor adhesion cannot provide sufficient protection to the substrates. The adhesion between coating and CRA's substrate strongly depends on a catalytic layer (nickel strike). It was found that both electroless and electrolytic coatings appeared to have no adhesion without the presence of a catalytic nickel layer. Carrying out repeated pull-off adhesion tests in this study showed a maximum value of 20 MPa for all the three coatings (Ni-P, Ni-P-Cu and Cu) until the adhesive failed. The pull-off adhesion test clearly showed that the adhesive bond between the coating and adhesive consistently failed, consequently the coatings always remained on the substrate during the friction test indicating good adhesion

between substrate and coating. Indeed, the surface free energy of coating decreases with the increase of copper content[28], which reduces the bonding between adhesive and coating, leading to failure of adhesive.

4.3 Micro-hardness

The micro-hardness of the coatings was measured using the Vickers scale and the results are given in Fig.5. Each coating was measured at three positions and the standard deviation of each coating is also shown on top of the corresponding bar. In the figure, the measurement for Ni-P-Cu coating was presented as the variable of copper concentration in the chemical bath, whilst 0g/L represents Ni-P. As a benchmark, the CRA's substrate is also presented in the figure, showing a value around 317 (corresponding to HRC34).

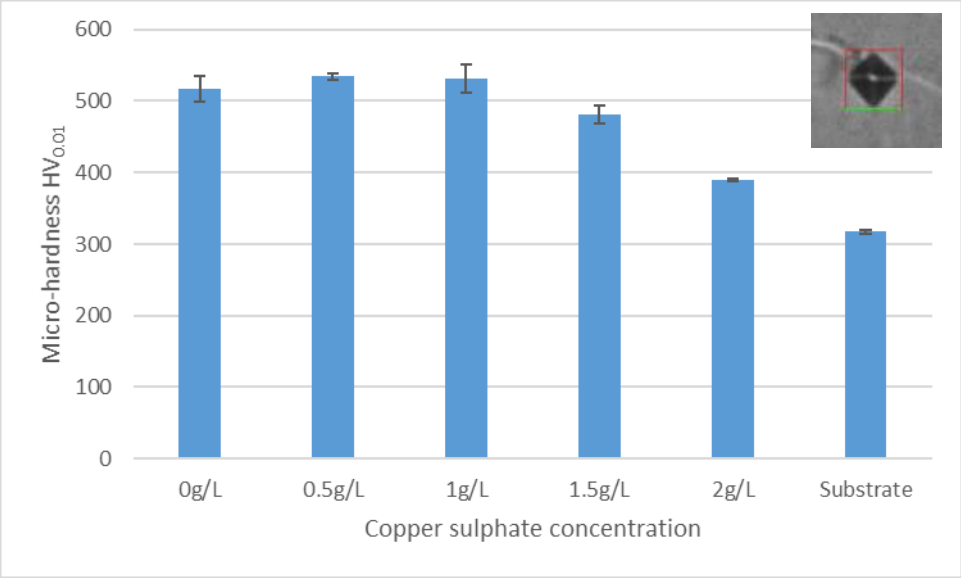

Fig.5. Comparison of micro-hardness for of electroless nickel coatings prepared by using various copper concentration in the chemical bath (substrate was $HV_{0.2}$ scale, while others were $HV_{0.01}$ scale). A typical image of imprint of indenter applied on Ni-P coating is also shown.

A very small change of micro-hardness can be seen when the copper sulphate concentration was relatively low (0-1 g/L), as the hardness was mainly controlled by the microstructure of the coating. With a high phosphorous content in the coating, the microstructure of coating was amorphous and showed a relatively low hardness. The micro-hardness decreased gradually when the copper sulphate concentration was over 1 g/L and showed a reduction by about 20% at 2 g/L. The dramatic reduction of micro-hardness indicated the change of microstructure of the deposited alloy of Ni-P-Cu due to the elevated copper content.

4.4 Coefficient of friction

The friction performance of different combinations of coating and lubricant were characterized by their CoF respectively. Fig.6 shows the dynamic change of CoF of a typical coating configuration during the friction test. The figure shows three cycles consisting of six strokes in total, the average CoF value for each stroke was calculated. It should be noted that the sliding direction changed during one cycle (tangential force flipped from positive to negative), therefore the calculation of coefficient of friction appeared negative value. Data shown in Fig.6 has been converted to absolute value. The value at the onset of each cycle is relatively small because of the lower contact pressure. At the end of each sliding stroke, friction rig dwelled for two seconds, showing a zero coefficient of friction at these gaps.

When lubricated by wet lubricants, the CoF of all the three coatings (Ni-P, Ni-P-Cu, Cu) fell into the range of 0.2-0.15, of which the combination of API dope and electrolytic copper coating (Cu/API) showed a relatively lower value (about 15% lower). It has been found that the friction performance of both the electroless nickel systems was benefitted by the shot-peening, showing a decrease of CoF, however, the shot-peening process did not help to improve the CoF of Cu/API system.

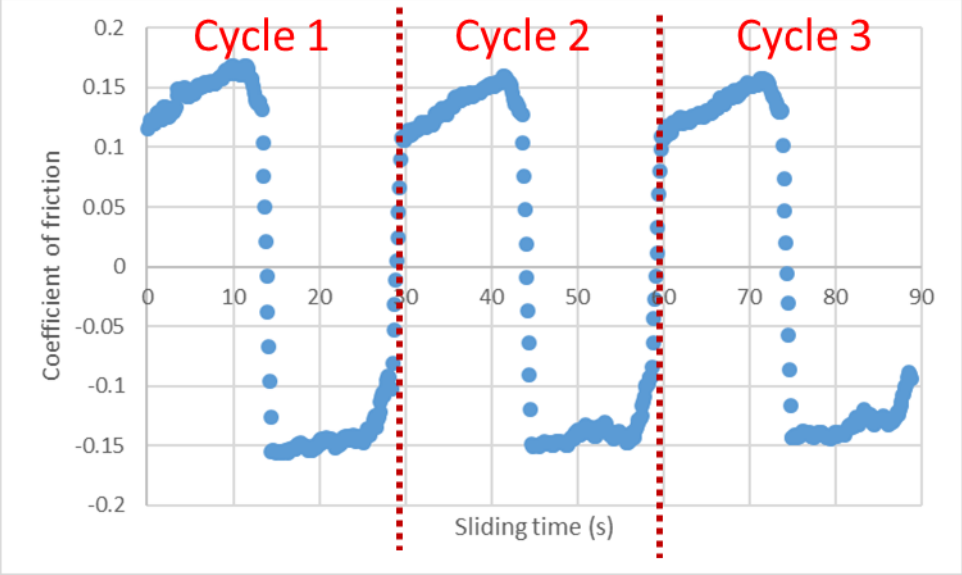

Fig.6. Dynamic change of CoF for three sliding cycles in the friction test (Ni-P coating with wet lubricant). The negative CoF indicates the change direction of tangential force due to the change of sliding direction.

Tin (Brinell hardness 51 MPa) and lead (Brinell hardness 38 MPa) are soft metals that can be burnished onto CRA's substrate without damaging the coatings. A very thin layer of tin and lead was burnished on the contact pair (both top and bottom samples in the friction rig) which helped to reduce the CoF significantly when shot-peening was applied to the test pins. This is because the surface profile had been modified by the shot-peening process so that the thin burnished metal layer acted like a semi-fluid film to prevent the direct hard contact between the contact pair during sliding as discussed in [29]. Due to the limit of the burnishing process, it is unlikely to obtain a thick metal layer, consequently, the burnished layer was easily worn. Indeed, the thickness of the burnished layer was thinner than the measurement capacity of a micro-meter (1 µm).

The presence of nanoparticles showed similar friction behaviour when compared to the burnishing process. The PTFE and WS_2 nanoparticles were dispersed as an aerosol and contained within a spray bottle. Nanoparticles remained on the surface just a few second after the solvent evaporated. It has been found that the friction performance was strongly dependant on the total amounts of PTFE and WS_2 nanoparticles on the surfaces of contact pair -- the nanoparticles can be removed from the surface after a very short sliding distance, particularly at higher contact pressure. Fig.7 shows a progressive increase in CoF when testing electroless Ni-P-Cu coating under high Hertzian contact stress (P_a =2 GPa) lubricated by PTFE and WS_2 nanoparticles.

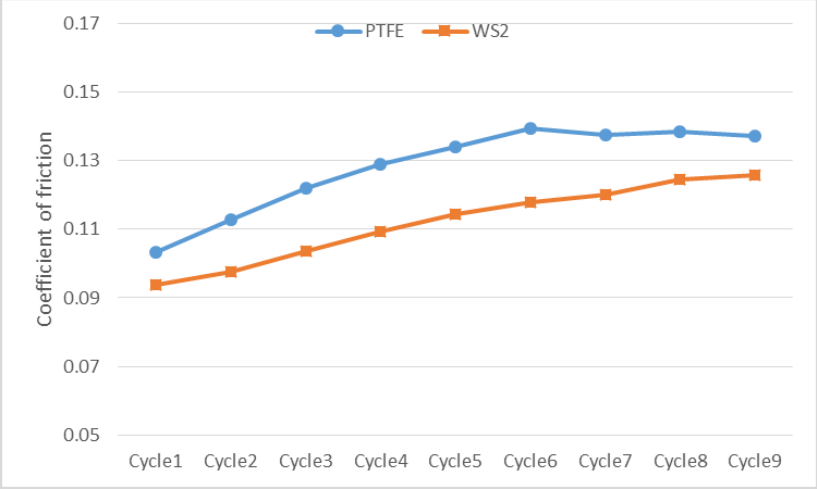

Fig.7. CoF for electroless Ni-P-Cu coating lubricated by PTFE and WS_2 nanoparticles. Both the top and bottom samples were shot-peened

There are nine sliding cycles in Fig.7, in which the nanoparticles lubricated the contact surfaces sufficiently at the very beginning of sliding under high contact pressure. However,

the CoF increased gradually whilst the sliding distance increased due to the removal of nanoparticles. It is interesting to note that the friction performance at high contact pressure showed an obvious improvement by increasing the amount of WS_2 nanoparticles but there was no change having increased PTFE nanoparticles. A closer inspection to the test pins indicated that the excessive PTFE nanoparticles coagulated and were removed completely from the contact region, whilst the WS_2 nanoparticles distributed uniformly on the surface.

It has been noticed that the shot-peening had helped to improve the friction behaviour of electroless nickel coatings, particularly when lubricated by nanoparticles, i.e. PTFE and WS_2. It has been found that the friction performance was highly dependent on the adhesion and distribution of the nanoparticles. Fig.8 shows the effects of tin burnishing prior to the application of nanoparticles on the CoF of the two electroless coatings. The PTFE nanoparticles formed solid condensed powder after a few seconds of spraying, which exhbited very poor adhesion on the tin burnished surface, therefore the PTFE condensed powder was mostly removed during sliding. As a contrast, the CoF was between 0.11 and 0.13. The application of sprayed WS_2 nanoparticles attached very well on the burnished surfaces so that galling was reduced to minimum, as discussed below, generating a much lower CoF.

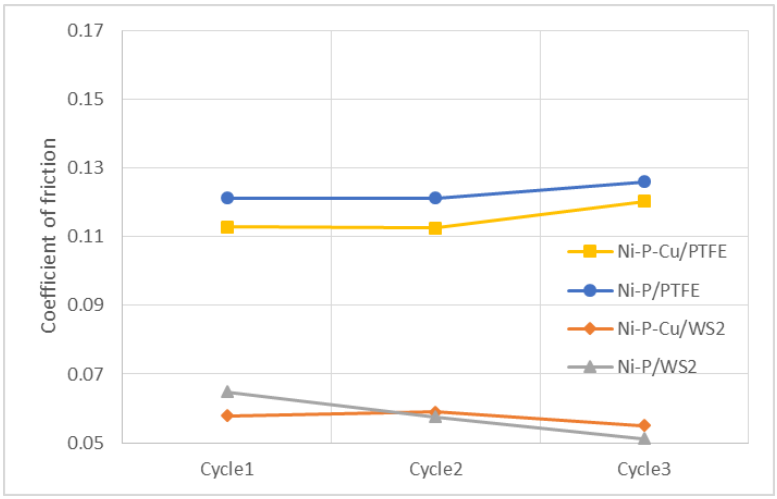

Fig.8. CoF for electroless Ni-P/Ni-P-Cu coatings lubricated with PTFE and WS_2 nanoparticles. Both the top and bottom test samples were shot-peened and burnished with tin. The friction tests were performed at high contact pressure (P_a =2 GPa).

In terms of CoF, there was no fundamental difference between electroless Ni-P and Ni-P-Cu, considering the friction tests under both intermediate and high contact pressures, however the corrosion resistance of Ni-P-Cu has been reported to be considerably better than Ni-P[30, 31]. For the electroless systems, the CoF increased about 15% by increasing the contact pressure

from intermediate (P_a=1.4 GPa) to high level (P_a=2 GPa). In order to validate the durability of coatings at high level of contact stress, an extensional friction test with nine sliding cycles (P_a=2GPa) were performed and the CoF of these lubricants were stable at the range of 0.13 to 0.15, as shown in Fig.9.

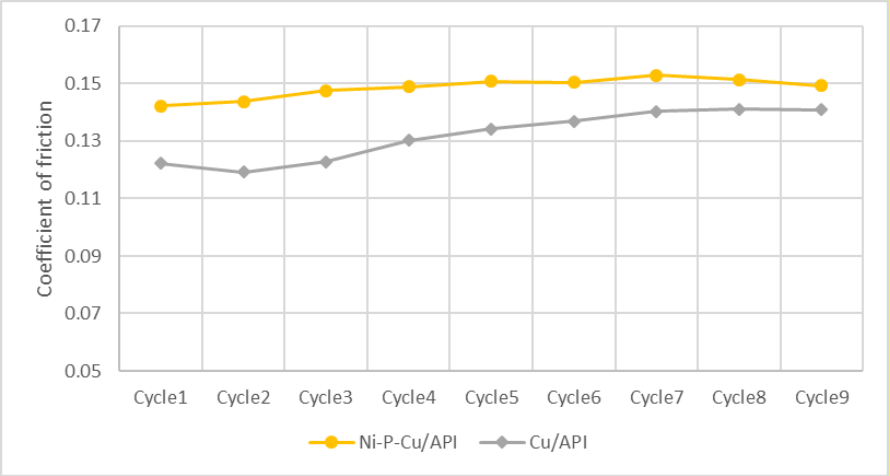

Fig.9. Testing electroless and electrolytic coatings lubricated by wet lubricants. Both the top and bottom samples were shot-peened.

A closer inspection into each stroke of the sliding cycles indicated a linear relationship between contact stress and CoF (the slope is designated as 'k'). Two regimes can be identified for the forward strokes (1+, 2+, 3+…) and backward strokes (1-, 2-, 3-…), corresponding to loading (makeup) and unloading (breakout). In the 'makeup' regime, the CoF increased linearly to the contact pressure, whilst the CoF became relatively stabilized in the 'breakout' regime.

4.5 Wear scar

Typical images of wear scar on the coating (bottom test sample) and indentation on the contact counterpart (bottom test sample) for three coatings are shown in Fig.10. The appearance of indentation at the contact area of the counterpart of Ni-P and Ni-P-Cu coatings looked similar (around 0.86mm in diameter), as a contrast, the diameter of indentation corresponding to copper coating was considerably smaller (0.66mm) due to a much lower micro-hardness. The wear scar on the coatings showed an opposite trend: the harder the coating, the lighter wear scar. The characteristic of anti-galling property of coatings should be the balance of wear scar and indentation.

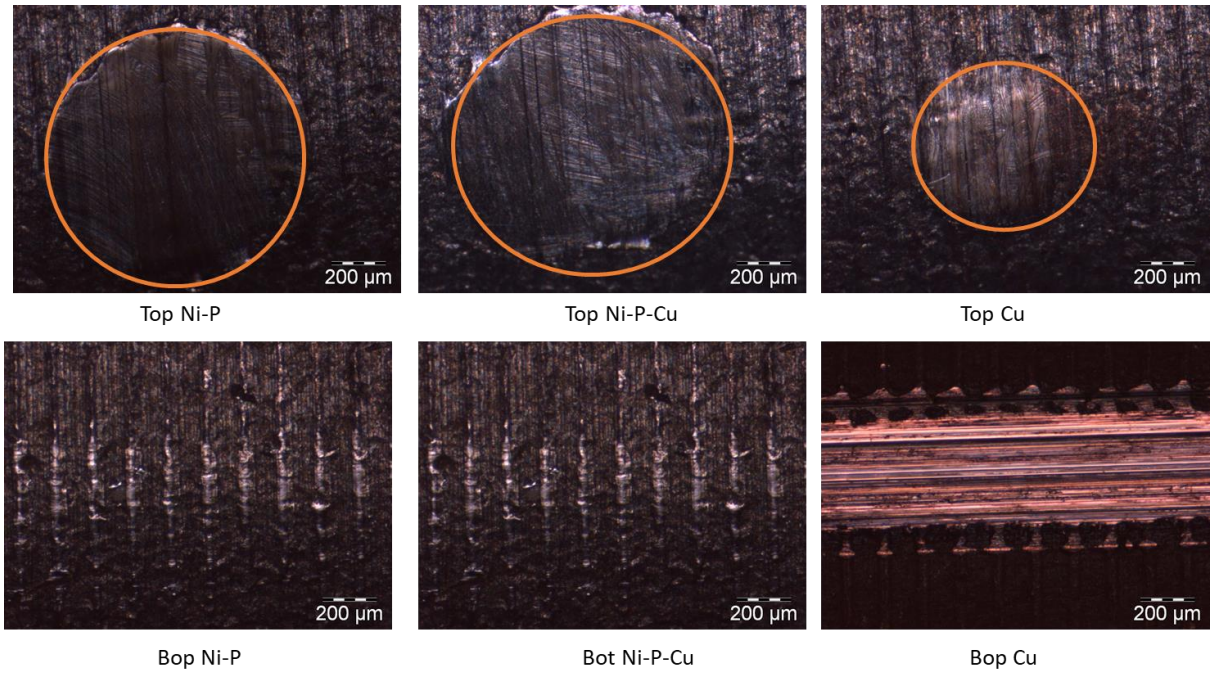

Fig.10. Comparison of wear scar and indentation of three coatings after three sliding cycles (270mm) at high Hertzian contact pressure (P_a=2 GPa)

As illustrated in Fig.1, neglecting the sliding wear, the indentation of a pair of perpendicular crossed cylinders is an approximate circle, of which the radius can be estimated by contact mechanics[32],

$$r = \sqrt[3]{\frac{3FR}{4E^*}} \qquad (3)$$

$$E^* = \frac{E}{2(1-\nu^2)}$$

where F is the normal force; R is the radius; and E and ν are elastic modulus and Poisson's ratio.

Substituting the material property and geometry into the equation, the diameters of indentation are calculated as 0.41mm and 0.53mm when the normal forces were 200N and 450N respectively, generating 1.5GPa and 2GPa Hertzian contact stress. If it is assumed that the indentation is a perfect circle, the depth of indentation can be calculated by the geometric relationship,

$$d = R - \sqrt{R^2 - r^2} \qquad (4)$$

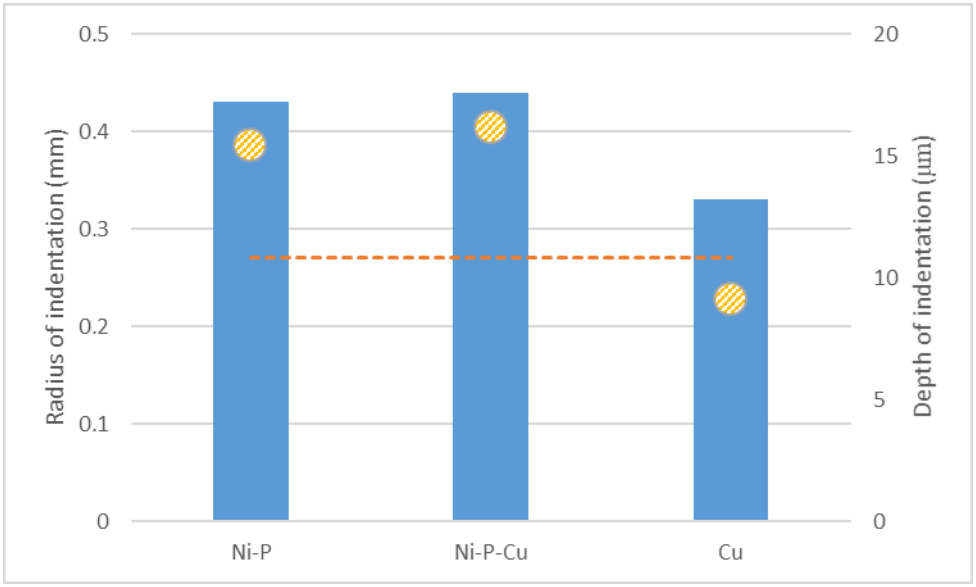

Fig.11. Radius and depth of wear scar on three coatings after three sliding cycles (total distance 270mm) at high Hertzian contact pressure (P_a=2GPa). Bar chart: measured wear scar radius (left scale); scatter balls: depth of indentation (right scale); dash line: prediction of wear scar radius by Equation 3 (left scale).

A measurement for radius of indentation was carried out by an optical microscope following sliding wear, and the results showed a much larger value compared to the prediction by Equation 3. Fig.11 gives a comparison of the radius of wear scar (r, bar chart) and the depth of indentation (d, scatter balls) for the three coatings. The predicted radius of wear scar is also shown in the figure as flat dash line. The measurement of the wear scar radius against electroless Ni-P and Ni-P-Cu coatings was about 40% higher than the prediction of Hertzian model. Though wear scar in the test against Cu coating was considerably smaller, the absolute value was still 18% higher than the prediction. This indicates a higher wear rate of the top sample against Ni-P and Ni-P-Cu coatings than much softer Cu coating. Note that the Hertzian model is based on the static condition and does not take into account the effects of the coating's micro-hardness. Considering the material hardness and sliding condition, the depth of indentation d_w is calculated by abrasive wear mechanics[33],

$$d_w = \frac{KP_aL}{H} \qquad (5)$$

Where K is non-dimensional constant; P_a is contact stress; L is sliding distance; and H is the material hardness. In this equation, the depth of indentation is proportional to the sliding distance. It is inferred that K constant for tests against Ni-P and Ni-P-Cu is higher than that

against Cu. However, after a careful inspection by optical microscope, no obvious change of depth of indentation and diameter of wear scar was observed following 3, 6 and 9 cycles of sliding (corresponding to 270mm, 540mm, and 810mm). One probable reason is that the asperities of both contact pair were burnished at the very beginning of sliding, leading to a stable CoF in the following sliding cycles (refer to section 4.3).

5. Conclusions

This paper has addressed the tribological testing for the investigation of electroless Ni-P and Ni-P-Cu coatings on CRA's based on a cross cylinder friction and galling rig. Friction tests were carried out at intermediate (1.5GPa) and high (2GPa) Hertzian contact stress, various surface pre-treatments and lubricating conditions were examined. Based on the experimental investigation some new findings can be concluded from this study.

In terms of tribological properties, the binary and ternary electroless coatings (Ni-P, Ni-P-Cu) presented similar behaviours such as CoF and wear scar, regardless of copper content within the coating alloy, which was very different from their anti-corrosion properties of the two coatings. Shot-peening showed a promising improvement to the tribological performance of the electroless coatings, but had a negative effect on the commercial coating system, i.e. electrolytic copper/API dope (Cu/API). The shot-peening particularly worked well when the electroless coatings were burnished by tin and lubricated by WS_2 nanoparticles.

In this study, the anti-galling properties were characterized by CoF, wear scar on coating and depth of indentation of contact counterpart. It was found that the wear scar and depth of indentation were considerably higher (approximate 40%) than the prediction of static Hertzian contact model. These factors of electroless coatings tended to be stable after a small sliding distance compared to an increasing trend of Cu/API, indicating a more durable service life for electroless coatings.

In this study the CoF of sliding cycles were decomposed as forward/backward strokes, which were classified as 'makeup' and 'breakout' regimes. It was found that there was a linear relation between CoF and contact stress for both regimes.

Acknowledgement

The authors would like to acknowledge Graham Souch, Sue Elliott, Peter Bond and Terry Richards for their support and expertise in the use of the various measuring equipment used to characterise the various coatings.

Reference

[1]. P. Rhodes, *Environment-assisted cracking of corrosion-resistant alloys in oil and gas production environments: a review.* Corrosion, 2001. **57**(11): p. 923-966.

[2]. A. Contreras, S. Hernández, R. Orozco-Cruz, and R. Galvan-Martínez, *Mechanical and environmental effects on stress corrosion cracking of low carbon pipeline steel in a soil solution.* Materials & Design, 2012. **35**: p. 281-289.

[3]. M. Ueda, K. Nakamura, N. Hudson, M. Z. Ibrahim, K. Selamat, and P. Chen. *Corrosion behavior of super 13Cr martensitic stainless steels in completion fluids*. in *CORROSION 2003*. 2003. NACE International.

[4]. H. Hoffmeister, *Modeling the effect of chloride content on hydrogen sulfide corrosion of pure iron by coupling of phase and polarization behavior.* Corrosion, 2008. **64**(6): p. 483-495.

[5]. E. E. Zúñiga, M. V. Rodríguez, V. R. Cruz, and J. U. Chavarín, *Effect of pH on carbon steel corrosion in the presence of a sour medium.* Superficies y Vacío, 2012. **25**(2): p. 139-145.

[6]. B. D. Craig, *Selection guidelines for corrosion resistant alloys in the oil and gas industry.* Chemical engineering world, 1998. **33**: p. 57-60.

[7]. B. D. Craig and L. Smith, *Corrosion Resistant Alloys (CRAs) in the oil and gas industry.* Nickel Institute Technical Series, 2011(1): p. 0073.

[8]. Q. Zhao and Y. Liu, *Comparisons of corrosion rates of Ni–P based composite coatings in HCl and NaCl solutions.* Corrosion Science, 2005. **47**(11): p. 2807-2815.

[9]. C. Gu, J. Lian, G. Li, L. Niu, and Z. Jiang, *High corrosion-resistant Ni–P/Ni/Ni–P multilayer coatings on steel.* Surface and Coatings Technology, 2005. **197**(1): p. 61-67.

[10]. P. Sahoo and S. K. Das, *Tribology of electroless nickel coatings – A review.* Materials & Design, 2011. **32**(4): p. 1760-1775.

[11]. H. Zhang, J. Zou, N. Lin, and B. I. N. Tang, *Review on electroless Ni-P coatings for improving surface performance of steel.* Surface Review and Letters, 2014. **21**(04): p. 1430002.

[12]. P. Sahoo and S. K. Das, *Tribology of electroless nickel coatings–a review.* Materials & Design, 2011. **32**(4): p. 1760-1775.

[13]. M. Palaniappa and S. Seshadri, *Friction and wear behavior of electroless Ni–P and Ni–W–P alloy coatings.* Wear, 2008. **265**(5-6): p. 735-740.

[14]. Z.-h. Li, Z.-y. Chen, S.-s. Liu, F. Zheng, and A.-g. Dai, *Corrosion and wear properties of electroless Ni-P plating layer on AZ91D magnesium alloy.* Transactions of Nonferrous Metals Society of China, 2008. **18**(4): p. 819-824.

[15]. P. Sahoo, *Wear behaviour of electroless Ni–P coatings and optimization of process parameters using Taguchi method.* Materials & Design, 2009. **30**(4): p. 1341-1349.

[16]. J. W. Jappes, B. Ramamoorthy, and P. K. Nair, *Novel approaches on the study of wear performance of electroless Ni–P/diamond composite deposites.* Journal of materials processing technology, 2009. **209**(2): p. 1004-1010.

[17]. A. Brenner; and G. Riddell, *1947 Deposition of nickel and cobalt by chemical reduction.* 1947.

[18]. F. Stewart, H. Le, J. Williams, A. Leech, B. Bezensek, and A. Roberts, *Characterisation of friction and lubrication regimes in premium tubular connections.* Tribology International, 2012. **53**: p. 159-166.

[19]. J. A. Williams and R. S. Dwyer-Joyce, *Contact between solid surfaces.* Modern tribology handbook, 2001. **1**: p. 121-162.

[20]. S. Takahashi, M. Hashimoto, and Y. Hirose, *An X-Ray study of shot peening material during fatigue.* JCPDS-International Centre for Diffraction Data, Advances in X-ray Analysis, 2000. **43**: p. 117-122.

[21]. P. Fu, C. Jiang, Z. Zhang, and V. Ji, *Residual stress and micro-structure of GCr15 steel after multistep shot peening.* Surface Engineering, 2014. **30**(11): p. 847-851.

[22]. G. Mallory, *The Fundamental Aspects of electroless nickel plating.*

[23]. P. Bindra and J. R. White, *Fundamental aspects of electroless copper plating.* Electroless Plating Fundamentals & Applications (Jan. 1990) pp, 1990: p. 289-375.

[24]. G. Salvago and P. Cavallotti, *CHARACTERISTICS OF THE CHEMICAL REDUCTION OF NI ALLOYS WITH HYPOPHOSPHITE.* Plating, 1972. **59**(7): p. 665-671.
[25]. H.-S. Yu, S.-F. Luo, and Y.-R. Wang, *A comparative study on the crystallization behavior of electroless Ni · P and Ni · Cu · P deposits.* Surface and coatings technology, 2001. **148**(2-3): p. 143-148.
[26]. G. Liu, L. Yang, L. Wang, S. Wang, L. Chongyang, and J. Wang, *Corrosion behavior of electroless deposited Ni–Cu–P coating in flue gas condensate.* Surface and coatings technology, 2010. **204**(21-22): p. 3382-3386.
[27]. R. Parkinson, *Properties and applications of electroless nickel.* Nickel Development Institute, 1997. **37**.
[28]. Y. H. Cheng, S. S. Chen, T. C. Jen, Z. C. Zhu, and Y. X. Peng, *Effect of copper addition on the properties of electroless Ni-Cu-P coating on heat transfer surface.* The International Journal of Advanced Manufacturing Technology, 2015. **76**(9): p. 2209-2215.
[29]. H. Le, F. Stewart, and J. Williams, *A Simplified Model of Surface Burnishing and Friction in Repeated Make-up of Premium Tubular Connections.* 2015.
[30]. H. Ashassi-Sorkhabi, H. Dolati, N. Parvini-Ahmadi, and J. Manzoori, *Electroless deposition of Ni–Cu–P alloy and study of the influences of some parameters on the properties of deposits.* Applied surface science, 2002. **185**(3-4): p. 155-160.
[31]. Y. Liu and Q. Zhao, *Study of electroless Ni–Cu–P coatings and their anti-corrosion properties.* Applied Surface Science, 2004. **228**(1-4): p. 57-62.
[32]. D. A. Hanaor, Y. Gan, and I. Einav, *Contact mechanics of fractal surfaces by spline assisted discretisation.* International Journal of Solids and Structures, 2015. **59**: p. 121-131.
[33]. I. Hutchings and P. Shipway, *Tribology: friction and wear of engineering materials*. 2017: Butterworth-Heinemann.